Analytical and Bioanalytical Chemistry (2025) 417:3127–3139
https://doi.org/10.1007/s00216-025-05852-w

RESEARCH PAPER

# A hemicyanine-based dual-responsive fluorescent sensor for the detection of lithium and cyanide ions: application in living cells

**Ziya Aydin[1] · Mukaddes Keskinates[2] · Esra Armagan[3] · Bahar Yilmaz Altinok[4] · Mevlut Bayrakci[4]**

Received: 7 December 2024 / Revised: 22 February 2025 / Accepted: 19 March 2025 / Published online: 3 April 2025


## Abstract

A hemicyanine-based colorimetric and fluorometric sensor, 2-(2-(2,3,5,6,8,9-hexahydrobenzo[b][1,4,7,10]tetraoxacyclododecin-12-yl)vinyl)-3,3-dimethyl-1-propyl-3H-indol-1-ium iodide (MH-5), was developed and synthesized to detect $Li^+$ and $CN^-$ ions in DMSO-PBS buffer solution (10 mM, pH 7.25, v/v 1:9). MH-5 displayed a rapid and highly selective colorimetric response to both $Li^+$ and $CN^-$, indicated by a distinct color change from pink to pale pink in the presence of $Li^+$ and to colorless upon $CN^-$ detection, without interference from other cations or anions. The interaction mechanisms of MH-5 with $Li^+$ and $CN^-$ ions were investigated using various analytical techniques, including $^1$H NMR, ESI–MS, FT-IR spectroscopy, and Job's plot analysis. These studies suggest that $CN^-$ is detected through nucleophilic addition to the indolium moiety of MH-5, while $Li^+$ detection occurs via coordination with oxygen atoms in the crown ether structure. The fluorescence-based detection limits for $Li^+$ and $CN^-$ were determined to be 0.150 µM and 0.154 µM, respectively. Additionally, MH-5 was evaluated in living cells, demonstrating effective cell penetration and reliable detection of $Li^+$ and $CN^-$ ions for potential bio-imaging applications.

**Keywords** Bio-imaging · Chemosensor · Cyanide · Dual-response · Fluorescence · Lithium ions

## Introduction

Detection of cations and anions has been an important part of modern research due to its widespread applications in biological, chemical, and environmental analysis. Among anions, cyanide ($CN^-$) is highly toxic to living organisms due to its strong affinity for binding to the heme group, which disrupts the function of cytochrome c oxidase, inhibiting the process of cellular respiration [1, 2]. This disruption leads to symptoms such as vomiting, seizures, loss of consciousness, and ultimately death. The lethal dose of $CN^-$ for humans can range from 0.5 to 3.5 mg per kg of body weight [3]. According to the World Health Organization (WHO), the maximum allowable cyanide concentration in drinking water is 1.9 µM [4]. Despite its toxicity, cyanide is widely used in industrial applications, producing high cyanide content in materials such as paper, textiles, and plastics. Furthermore, some biological processes in bacteria and fungi release cyanide [5, 6]. However, the accidental release of cyanide poses significant environmental and health risks. Therefore, developing efficient, cost-effective methods for cyanide detection is critical.

Among cations, lithium ($Li^+$) is one of the most biologically important alkali cations, and lithium-containing drug preparations are routinely used in medical and clinical applications for the treatment of bipolar disorders and manic-depressive psychosis [7–9]; also, there is interest in lithium salts for the treatment of amyotrophic lateral sclerosis (ALS) and Alzheimer's disease [10]. Lithium plays a vital role in energy storage technologies, particularly

✉ Ziya Aydin
ziyaaydin@kmu.edu.tr

✉ Mevlut Bayrakci
mevlutbayrakci@gmail.com; mbayrakci@kmu.edu.tr

[1] Vocational School of Technical Sciences, Karamanoglu Mehmetbey University, 70100 Karaman, Turkey

[2] Department of Environmental Protection Technologies, Kazım Karabekir Vocational School, Karamanoglu Mehmetbey University, 70100 Karaman, Turkey

[3] Department of Pharmacy Services, Ermenek Uysal and Hasan Kalan Health Services Vocational School, Karamanoglu Mehmetbey University, 70400 Karaman, Turkey

[4] Department of Bioengineering, Faculty of Engineering, Karamanoglu Mehmetbey University, 70200 Karaman, Turkey

in batteries, and its demand is experiencing significant growth [11, 12]. Although the extensive use of lithium has contributed to reducing environmental pollution associated with conventional energy sources, it also poses serious risks. For instance, lithium present in discarded cathode materials can adversely affect human health by leaching into the soil and accumulating in the food chain, leading to potential kidney damage and nephrotic syndrome [13]. Consequently, there is an urgent need to develop and selective methods for the detecting $Li^+$ cations.

Over the past few decades, a range of analytical techniques, such as atomic absorption spectroscopy [14, 15], voltammetry [16, 17], and electrochemical detection [4, 18], have been employed for the detection of $Li^+$ and $CN^-$ ions. However, fluorimetric techniques have garnered significant attention due to their simplicity, high sensitivity, and selectivity compared to these traditional methods [19–24]. Consequently, developing a chemosensor capable of providing a reliable and effective response to $Li^+$ and $CN^-$ has become a topic of increasing interest in recent studies.

Due to the dedicated efforts of researchers, numerous effective colorimetric and fluorescent sensors have been developed for the selective detection of $CN^-$, primarily utilizing mechanisms such as designs involving nanoparticles [25], nucleophilic addition [26], and metal complex ensemble displacement [27, 28]. Among these, sensors based on nucleophilic reactions with functional groups like pyridinium rings [29, 30], dicyano-vinyl [31, 32], and indolium groups [33–37] have demonstrated notable selectivity, attributed to $CN^-$, high nucleophilicity. Recently, indolium has shown particular promise as a reactive group for $CN^-$ detection due to its positive charge, which creates a strong electrostatic attraction with $CN^-$.

In recent literature, various sensors for $Li^+$ ions have been developed, typically utilizing chelation-induced photophysical changes, such as photoinduced electron transfer (PET) [38], intramolecular charge transfer (ICT) [39], and Förster resonance energy transfer (FRET) [40]. To construct optical sensors, chemists typically design a system comprising two main components: an ionophore that selectively binds lithium and a chromophore or fluorophore responsible for optical changes [41, 42]. Numerous ligands capable of forming lithium chelates have been explored, including porphyrins [43, 44], phenanthrolines [45], and calixarenes [46, 47], but crown ethers and their derivatives [39, 48–51] are especially known for their strong affinity for lithium. Chromo- and fluorophores used in these systems are often small molecular dyes such as BODIPY [50], coumarins [52], and naphthalimides [38]. When functionalized with crown ethers, these probes generally exhibit complex molecular architectures that require multiple synthetic steps to prepare; however, they offer high selectivity for $Li^+$.

With this background and our interest in dual-responsive fluorescent sensors, we decided to study on a turn-off fluorescent, MH-5, synthesized by combining2,3,3-trimethyl-1-propyl-3H-indol-1-ium iodide (the indole moiety) and 2,3,5,6,8,9-hexahydrobenzo[b][1, 4, 7, 10] tetraoxacyclododecine-12-carbaldehyde (the crown ether moiety), for the detection of $Li^+$ and $CN^-$. The optical and colorimetric properties of the sensor were examined using naked eye observation, fluorescence, and UV–Vis spectrophotometry in DMSO-PBS buffer (10 mM, pH = 7.25, v/v, 1:9). The sensor demonstrated rapid and highly selective detection of $Li^+$ and $CN^-$ ions among the tested cations and anions. Spectrophotometric methods were employed to analyze the interactions between MH-5 and $Li^+$/$CN^-$, with $^{13}C$ NMR titration experiments used to clarify the sensing mechanism for $CN^-$ and FT-IR experiments for $Li^+$. The sensor was further tested for bio-imaging of $Li^+$ and $CN^-$ in living cells for practical applications.

## Experimental

### Materials and instruments

All solvents and reagents were of analytical reagent grade and were used without further purification. 2,3,3-Trimethyl-3H-indole, 1-iodopropane, 3,4-dihydroxybenzaldehyde, p-Toluene sulfonyl chloride, and triethylene glycol were purchased from Sigma-Aldrich. The metal salts and the anion salts were commercially obtained from Acros Organics or Sigma-Aldrich.

$^{13}C$ NMR and $^1H$ NMR spectra were acquired using an Agilent Premium Compact spectrometer operating at 600 MHz at a temperature of 298 K. Infrared (IR) spectra were recorded using a Bruker Vertex FT-IR spectrometer with ATR (Attenuated Total Reflectance) capabilities. UV–Vis absorption and fluorescence emission spectra were measured with a Shimadzu UV-1800 spectrophotometer and a Hitachi F-7100 spectrophotometer, respectively, both at 298 K. For cellular imaging experiments, a Leica™ DM 3000 fluorescence microscope was employed to capture cell images.

### Synthesis of 2-(2-(2,3,5,6,8,9-hexahydrobenzo[b][1,4,7,10]tetraoxacyclododecin-12-yl)vinyl)−3,3-dimethyl-1-propyl-3H-indol-1-ium iodide (MH-5)

2,3,3-Trimethyl-1-propyl-3H-indol-1-ium iodide and 2,3,5,6,8,9-hexahydrobenzo[b][1, 4, 7, 10]tetraoxacyclododecine-12-carbaldehyde was synthesized as reported in the literature [53, 54] (also see Electronic Supplementary Material Scheme S1).

2,3,3-Trimethyl-1-propyl-3H-indol-1-ium iodide (**C1**) (0.330 g, 1 mmol) and 2,3,5,6,8,9-hexahydrobenzo[b][1, 4, 7,

10]tetraoxacyclododecine-12-carbaldehyde (**C2**) (0.250 g, 1 mmol) were dissolved in 5.0 mL of ethanol. The mixture was stirred at 100 °C for 1 h. When the substances were completely dissolved, 20 µL (2 drops) of piperidine was added. The mixture was refluxed at 100 °C for 12 h (checked by TLC). After cooling to room temperature, it was kept in the refrigerator at − 20 °C for 1 day. The resulting precipitate was collected by filtration. It was washed with cold ethanol and dried in a vacuum oven. 0.230 g of dark purple MH-5 was obtained (41%). $^{1}$H NMR (600 MHz, DMSO) δ 7.47–7.30 (5H), 7.05 (m, 1H), 6.85 (dd, $J$ = 17.1, 4.7 Hz, 2H), 6.06 (s, 1H), 4.83 (d, $J$ = 3.3 Hz, 2H), 3.68–3.54 (m, 12H), 2.10 (dd, $J$ = 15.1, 8.3 Hz, 2H), 2.02 (s, 6H), 1.12 (t, $J$ = 10.8 Hz, 3H). $^{13}$C NMR (DMSO-d6, 150 MHz), δ (ppm): 180.0, 161.8, 154.8, 153.4,143.2, 141.4, 129.0, 128.0, 123.2, 122.8, 114.0, 112.9, 105.2, 70.7, 70.1, 68.3, 52.7, 44.1, 26.9, 22.1, 11.0. MALDI-Tof: $C_{27}H_{34}NO_4^+$ ([M]$^+$ without I$^-$) found 436.466, calculated 436.245.

## General procedure for detecting spectra

Stock solution of MH-5 was prepared at a concentration of 1.0 mM in dimethyl sulfoxide (DMSO). This solution was further diluted to achieve a final sensor concentration of 1 µM using DMSO-PBS buffer (10 mM, pH = 7.25, v/v, 1:9) solvent system for spectroscopic analysis. Stock solutions of metal ions (10 mM) were prepared using various salts, including $AlCl_3{\cdot}6H_2O$, $AgNO_3$, $CaCl_2$, $CoCl_2{\cdot}6H_2O$, $3CdSO_4{\cdot}8H_2O$, $CuCl_2{\cdot}2H_2O$, $CrCl_3{\cdot}6H_2O$, $HgCl_2$, $FeCl_3{\cdot}6H_2O$, $MgCl_2{\cdot}6H_2O$, KCl, $Mn(NO_3)_2{\cdot}4H_2O$, NaCl, $Ni(NO_3)_2{\cdot}6H_2O$, $Pb(NO_3)_2$, $LiNO_3$, and $ZnCl_2$, all of which were dissolved in deionized water. Stock solutions (10 mM) of the tetrabutylammonium salts of $CN^-$, $SCN^-$, $HPO_4^{2-}$, $Cl^-$, $AcO^-$, $I^-$, $CO_3^{2-}$, $H_2PO_4^-$, $NO_3^-$, $ClO_4^-$, $NO_2^-$, $SO_3^{2-}$, $OH^-$, $SO_4^{2-}$, and $Br^-$ were prepared in DMSO. Stock solution (10 mM) of sodium salt of $PO_4^{3-}$ was prepared in $H_2O$. UV–Vis absorption spectra of MH-5 were recorded using a quartz cuvette with a 1-cm path length over the 300–800 nm wavelength range, both in the presence and absence of the metal ions and the anions tested. Fluorescence emission spectra were obtained by exciting the samples at a wavelength of 530 nm and measuring emissions between 550 and 600 nm using a 3.0-mL cuvette. All spectroscopic measurements were conducted under consistent conditions at room temperature, with spectra collected 5 min after the addition of each metal ion.

## General procedure for fluorescence microscopy imaging in cultured cells

### Cell culture

Colon adenocarcinoma cell line HT-29 was purchased from American Type Culture Collection. The HT-29 (human colorectal adenocarcinoma cell line) was cultured in RPMI (supplemented with 110 mg/L sodium pyruvate and 1 g/L glucose; Invitrogen, Gibco, Karlsruhe, Germany) containing 100 units/mL penicillin–streptomycin and gentamicin (0.01%). The L9-29 (epithelial cell line) was cultured in DMEM (4.5 g/L glucose; Gibco, Karlsruhe, Invitrogen, Germany) containing 100 units/mL penicillin/streptomycin and gentamicin (0.01%). All mediums were further supplemented with 10% fetal bovine serum (FBS) (Thermo Fisher Scientific). Cells were seeded in each well of uncoated 96-well microplates and incubated in a humidified atmosphere with 5% $CO_2$ at 37 °C for 18 h.

### Cell viability assay

The cytotoxicity of MH-5 in epithelial and cancer cell lines (L9-29 and HT-29) was evaluated using the Alamar Blue assay [55, 56]. Cells were cultured in DMEM and RPMI media at 37 °C in an atmosphere of 5% $CO_2$. After each cell line reached a density of $1 \times 10^4$ cells, they were harvested and seeded into a 96-well cell culture plate. Cells were then treated with 10 different concentrations (0.1 µM to 100 µM) of MH-5 and incubated for 18 h. Each sample was prepared in triplicate, with untreated cells as negative controls. After the 18-h incubation, Alamar Blue reagent (1:10, v/v) was added to each well and incubated for 4 h. Spectrophotometric measurements were taken at 570 nm and 600 nm. Cell viability for each sample was calculated, with the control wells set as 100%.

### Fluorescence imaging

Cells cultured in RPMI were treated with 10 mM $Li^+$ and $CN^-$ ion solutions (2 µL; final concentration: 20 µM) dissolved in sterilized PBS (pH 7.4) and incubated at 37 °C for 30 min. After treatment, the cells were washed with PBS (2 mL × 3) to remove residual ions. RPMI (2 mL) was added to the cell culture, followed by treatment with an MH-5 solution (2 µL; final concentration: 20 µM) dissolved in DMSO-PBS buffer. Samples were incubated at 37 °C for 30 min. The culture medium was then removed, and the treated cells were washed with PBS (2 mL × 3) before observation. Fluorescence imaging was performed using a Leica fluorescence microscope. The cells were excited with a red fluorescent light laser at 590 nm, and emission was collected at 615 ± 25 nm.

## Results and discussions

The synthesis of MH-5 was completed through a three-step reaction process. Initially, the starting compounds, 2,3,3-trimethyl-1-propyl-3H-indol-1-ium iodide and

2,3,5,6,8,9-hexahydrobenzo[b][1, 4, 7, 10]tetraoxacyclododecine-12-carbaldehyde [53, 54], were synthesized in the first and second steps. In the last step, these compounds were combined to yield MH-5. The structure of MH-5 was confirmed using NMR (both $^{1}H$ and $^{13}C$ NMR) and Q-TOF LC/MS mass spectrometry, with corresponding spectra provided in Figs. S1–S3 of the Electronic Supplementary Material. The synthetic pathway for MH-5 was illustrated in Scheme 1.

## Spectroscopic studies of MH-5 with cations

To determine the selectivity of MH-5, the color changes observable to the naked eye were initially tested by exposing MH-5 (5.0 μM) to various metal ions (5.0 μM), including $Li^+$, $Ag^+$, $Al^{3+}$, $Fe^{3+}$, $K^+$, $Ca^{2+}$, $Co^{2+}$, $Cd^{2+}$, $Hg^{2+}$, $Cu^{2+}$, $Mg^{2+}$, $Mn^{2+}$, $Na^+$, $Ni^{2+}$, $Pb^{2+}$, $Cr^{3+}$, and $Zn^{2+}$ in DMSO-PBS buffer (10 mM, pH 7.25, 1:9 v/v). Among all tested ions, only $Li^+$ triggered a noticeable color shift in MH-5 from pink to pale pink (see Electronic Supplementary Material Fig. S4). Correspondingly, UV–Vis spectra of MH-5 with these metal ions were obtained under conditions similar as to those of the naked eye detection tests. MH-5 alone (5.0 μM) showed a peak absorption at 550 nm ($\varepsilon = 7.80 \times 10^4$ $M^{-1}$ $cm^{-1}$). However, when $Li^+$ was added, the absorbance at 550 nm decreased significantly ($\varepsilon = 2.58 \times 10^4$ $M^{-1}$ $cm^{-1}$ at a 1:1 MH-5/$Li^+$ ratio). In contrast, other ions including $Ag^+$, $Al^{3+}$, $Fe^{3+}$, $K^+$, $Ca^{2+}$, $Co^{2+}$, $Cd^{2+}$, $Hg^{2+}$, $Cu^{2+}$, $Mg^{2+}$, $Mn^{2+}$, $Na^+$, $Ni^{2+}$, $Pb^{2+}$, $Cr^{3+}$, and $Zn^{2+}$ exhibited minimal responses, as shown by MH-5 analysis (Fig. 1a).

The metal ion selectivity of MH-5 was further evaluated using fluorescence spectroscopy. As shown in Fig. 1b, MH-5 exhibited a strong emission peak at 602 nm when excited at 530 nm, and the fluorescence quantum yield was calculated to be 0.096 [57]. Upon the addition of the metal ions tested, there was a slight quenching in fluorescence intensity at 602 nm; however, a substantial quenching effect (83%) was observed specifically with $Li^+$, resulting color change under UV-lamb (see Electronic Supplementary Material Fig. S5). The quantum yield value also changed to 0.034.

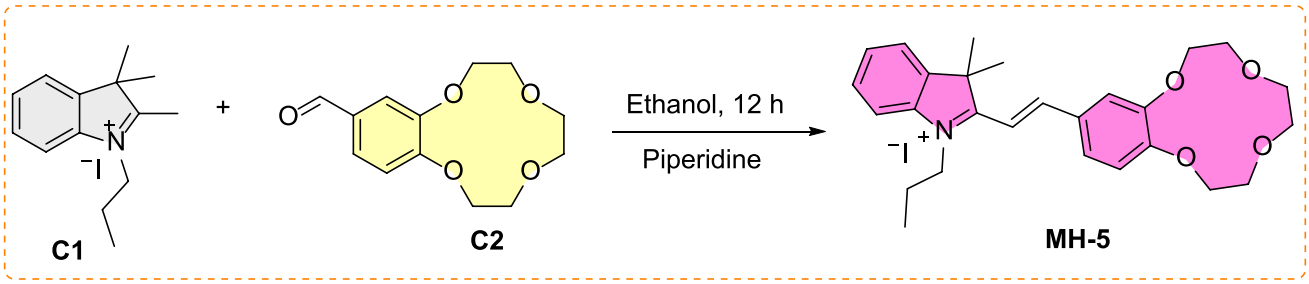


**Scheme 1.** Synthesis of the sensor, MH-5

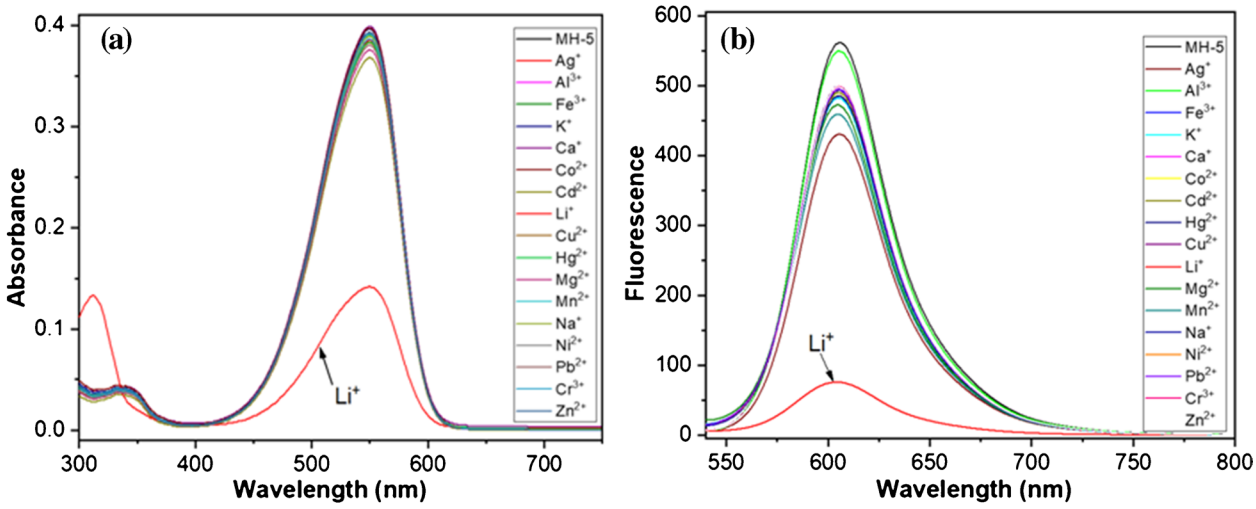


**Fig. 1** **a** Absorbance and **b** fluorescence spectra of 5.0 μM MH-5 to the metal ions tested (5.0 μM of $Ag^+$, $Al^{3+}$, $Fe^{3+}$, K+, $Ca^{2+}$, $Co^{2+}$, $Cd^{2+}$, $Hg^{2+}$, $Cu^{2+}$, $Li^+$, $Mg^{2+}$, $Mn^{2+}$, $Na^+$, $Ni^{2+}$, $Pb^{2+}$, $Cr^{3+}$, and $Zn^{2+}$) in DMSO-PBS buffer (10 mM, pH = 7.25, v/v, 1:9)

These findings from naked eye observation, absorption and fluorescence spectroscopy indicate that MH-5 serves as a highly selective colorimetric and on–off fluorescent sensor for detecting $Li^+$.

The time response of a fluorescence sensor is a crucial parameter for assessing its practical applicability. The kinetics of the interaction between MH-5 and $Li^+$ were examined in DMSO-PBS buffer solution (10 mM, pH 7.25, 1:9 v/v). As presented in Fig. S6 of the Electronic Supplementary Material, the emission intensity of MH-5 at 602 nm decreased rapidly upon the addition of 1.0 equivalent of $Li^+$, reaching a minimum value within 2 min and remaining stable over long reaction times. This rapid response highlights the potential of MH-5 as an efficient sensor, providing time-saving advantages and enhancing its applicability in practical settings.

In order to understand the optimal working condition of MH-5 and MH-5/$Li^+$, the effect of pH on selectivity was studied in the range of 3.5–10 pH. MH-5 showed no fluorescence response to hydrogen ions within a pH range of 3.5 to 9.0, indicating strong stability over a wide pH spectrum. In the presence of $Li^+$, fluorescence quenching was observed at 602 nm, with the fluorescence signal remaining stable from pH 3.5 to 8.0. These findings suggest that MH-5 is suitable for $Li^+$ detection within a pH range of 3.5 to 8.0, supporting its potential applicability in biological systems (see Electronic Supplementary Material Fig. S7).

Competition studies were also performed to assess the selective sensing behavior of MH-5 toward $Li^+$ in the presence of competing metal ions, including $Ag^+$, $Al^{+3}$, $Fe^{3+}$, $K^+$, $Ca^{2+}$, $Co^{2+}$, $Cd^{2+}$, $Hg^{2+}$, $Cu^{2+}$, $Li^+$, $Mg^{2+}$, $Mn^{2+}$, $Na^+$, $Ni^{2+}$, $Pb^{2+}$, $Cr^{3+}$, and $Zn^{2+}$. Upon adding 5.0 equivalents of these competing metal ions, a fluorescence quenching at 602 nm (indicated by blue bars) was observed following the subsequent addition of 5.0 equivalents of $Li^+$. These findings indicate that MH-5 can function as an effective $Li^+$ sensor even in the presence of various competing cations (Fig. 2).

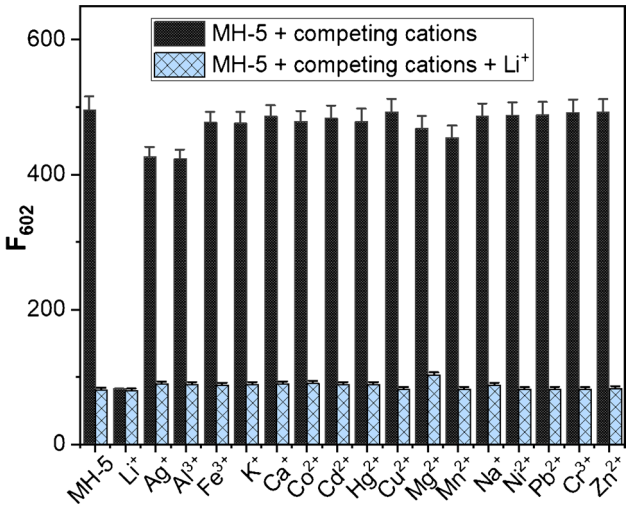


**Fig. 2** Fluorescence responses of 5.0 μM MH-5 to the presence of 50.0 μM metal ions tested (black bars) and the subsequent addition of $Li^+$ (blue bars) in DMSO-PBS buffer (10 mM, pH = 7.25, v/v, 1:9); the bars represent the fluorescence intensity at 602 nm (excitation wavelength was 530 nm)

## Spectroscopic studies of MH-5 with anions

The remarkable photophysical characteristics of MH-5 were further examined using absorbance and emission spectroscopy in the presence of the following anions in their tetrabutylammonium salts from $CN^-$, $Br^-$, $AcO^-$, $Cl^-$, $SO_3^{2-}$, $I^-$, $SO_4^{2-}$, $OH^-$, $NO_3^-$, $NO_2^-$, $ClO_4^-$, $HPO_4^{2-}$, $CO_3^{2-}$, and $H_2PO_4^-$ in DMSO-PBS buffer (10 mM, pH = 7.25, v/v, 1:9). As previously noted, MH-5 (5.0 μM) showed an absorption band with a molar absorptivity of $\varepsilon = 7.80 \times 10^4\ M^{-1}\ cm^{-1}$ at 550 nm. Upon the addition of $CN^-$ to the MH-5 solution, the color changed from pink to colorless (see Electronic Supplementary Material Fig. S8), and the absorbance intensity at 550 nm nearly disappeared (Fig. 3a). In contrast, the color and UV–VİS spectrum of MH-5 remained largely unchanged in the presence of other tested anions.

The fluorescence spectra of MH-5 were obtained both in the absence and presence of $CN^-$ in a DMSO-PBS buffer (10 mM, pH 7.25, 1:9 v/v). As illustrated in Fig. 3b, MH-5 (5.0 μM) exhibited strong fluorescence at 602 nm upon excitation at 530 nm, as mentioned above. While the addition of various anions resulted in a slight quenching of fluorescence intensity at 602 nm, a pronounced quenching effect (92%) was specifically observed with $CN^-$, accompanied by a visible color change under UV light (see Electronic Supplementary Material Fig. S9). The quantum yield value also changed to 0.019. These results from naked eye observation, absorption, and fluorescence spectroscopy demonstrate that MH-5 functions as a highly selective colorimetric and on–off fluorescent sensor for $CN^-$ detection.

The kinetic of the MH-5/$CN^-$ interaction system was also studied in DMSO-PBS buffer solution (10 mM, pH 7.25, v/v, 1:9). As shown in Fig. S10 of the Electronic Supplementary Material, the emission intensity of MH-5 at 602 nm rapidly decreased upon the addition of 1.0 equivalent of $CN^-$, reaching its minimum value within 5 min and remaining stable with extended reaction time. This property of MH-5 underscores its suitability as a highly efficient sensor, offering time-saving advantages and enhancing its utility for practical applications.

The effect of pH on $CN^-$ detection by MH-5 was evaluated through fluorescence spectroscopy. Fluorescence spectra of MH-5, both in the presence and absence of $CN^-$, were recorded across a pH range of 3.5 to 10 (see Electronic Supplementary Material Fig. S11). The sensor showed no

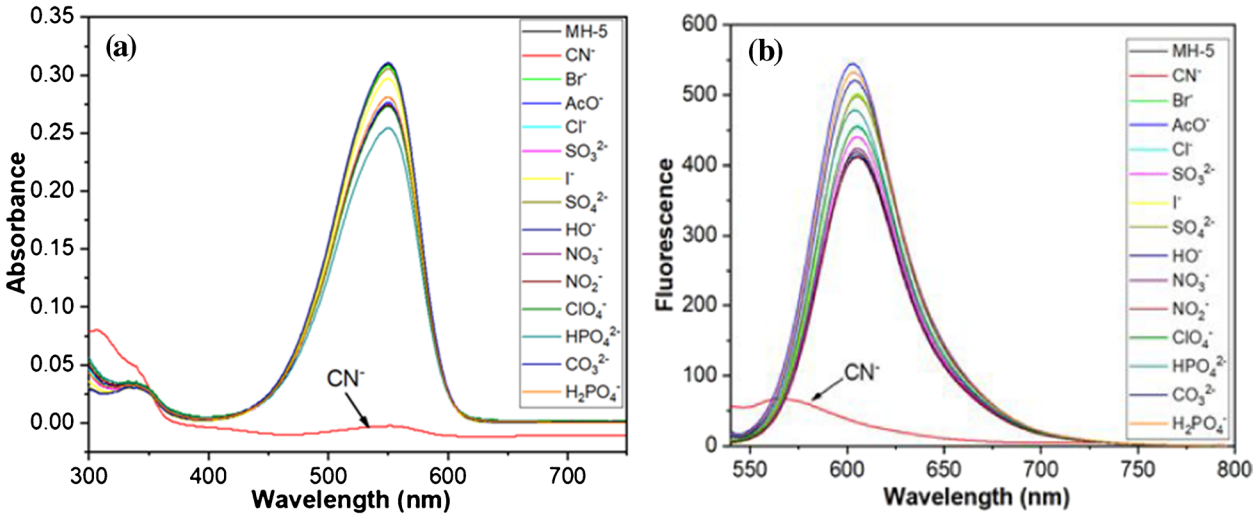


**Fig. 3** **a** Absorbance and **b** fluorescence spectra of 5.0 μM MH-5 to anions tested (5.0 μM of $CN^-$, $Br^-$, $AcO^-$, $Cl^-$, $SO_3^{2-}$, $I^-$, $SO_4^{2-}$, $OH^-$, $NO_3^-$, $NO_2^-$, $ClO_4^-$, $HPO_4^{2-}$, $CO_3^{2-}$, and $H_2PO_4^-$) in DMSO-PBS buffer (10 mM, pH = 7.25, v/v, 1:9)

response to hydrogen ions within a pH range of 3.5 to 9.0, indicating strong stability over a wide pH spectrum. In the presence of $CN^-$, fluorescence quenching was observed at 602 nm, with the fluorescence signal remaining stable from pH 3.5 to 10.0. These findings suggest that MH-5 is suitable for $CN^-$ detection within a pH range of 3.5 to 9.0, supporting its potential applicability in biological systems.

Competition studies were also performed to assess the selective sensing behavior of MH-5 toward $CN^-$ in the presence of competing anions, including $Br^-$, $AcO^-$, $Cl^-$, $SO_3^{2-}$, $I^-$, $SO_4^{2-}$, $OH^-$, $NO_3^-$, $NO_2^-$, $ClO_4^-$, $HPO_4^{2-}$, $CO_3^{2-}$, $H_2PO_4^-$, $PO_4^{3-}$, and $SCN^-$. Upon adding 5.0 equivalents of these competing anions, a fluorescence quenching at 602 nm (indicated by blue bars) was observed following the subsequent addition of 5.0 equivalents of $CN^-$. These findings indicate that MH-5 can function as an effective $CN^-$ sensor even in the presence of various competing anions (Fig. 4).

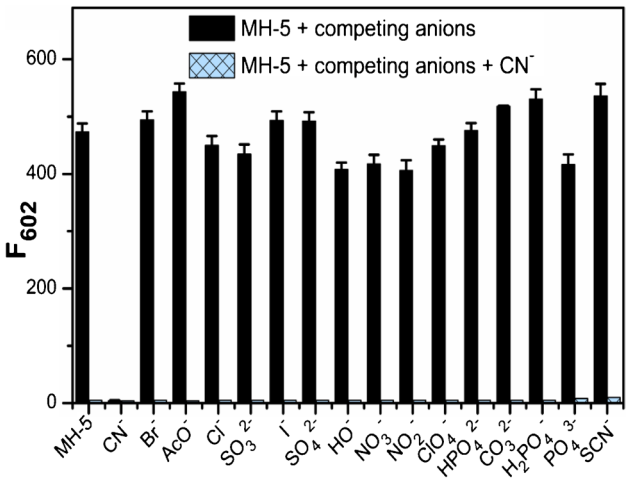


**Fig. 4** Fluorescence responses of 5.0 μM MH-5 to the presence of 50.0 μM anions tested (black bars) and the subsequent addition of $CN^-$ (blue bars) in DMSO-PBS buffer (10 mM, pH = 7.25, v/v, 1:9); the bars represent the fluorescence intensity at 602 nm (excitation wavelength was 530 nm)

## Proposed binding mode and sensing mechanisms

To elucidate the binding mode of MH-5 with $Li^+$ and $CN^-$, the binding stoichiometries for MH-5 with $Li^+$ and with $CN^-$ were initially examined. Various analytical techniques were employed to accurately determine the stoichiometry of interactions of MH-5 with $Li^+$ and $CN^-$, respectively. Job's plot, derived from UV–Vis spectroscopic measurements, exhibited a maximum absorption when the molar fraction of $Li^+$ and $CN^-$ reached approximately 0.5 (see Electronic Supplementary Material Fig. S12 and Fig. S13). This result suggests a 1:1 binding stoichiometry between MH-5 and both $Li^+$ and $CN^-$.

UV–Vis titration and fluorescence titration were also applied to study the binding stoichiometry between MH-5 and $Li^+$ and $CN^-$. As depicted in Fig. S14 and S15 of the Electronic Supplementary Material, the absorption intensity of MH-5 (5.0 μM) in DMSO-PBS buffer (10 mM, pH = 7.25, v/v, 1:9) at 550 nm gradually decreased upon the addition of $Li^+$ and $CN^-$ at varying concentrations, reaching saturation upon the addition of 1.0 equivalent of each ion. This behavior suggests a 1:1 stoichiometric interaction between MH-5 and both $Li^+$ and $CN^-$. Furthermore, clear isosbestic points were observed at 337 nm for $Li^+$ and 354 nm for $CN^-$, indicating a shift from the free form of MH-5 to the complexed forms MH-5 + $Li^+$ and MH-5 + $CN^-$as binding interactions occur [58]. Fluorescence titration experiments

also supported the 1:1 stoichiometry between MH-5 and both $Li^+$ and $CN^-$. As seen in Fig. 5a and 5b, the titration curve (a plot from fluorescence intensities versus $Li^+$ or $CN^-$ at various concentrations) decreased linearly, reaching saturation at 1:1 ratio of MH-5 between $Li^+$ and $CN^-$. This outcome is consistent with a 1:1 binding stoichiometry for both ions. MALDI-TOF mass results also supported a 1:1 ratio between MH-5 and $CN^-$ (see Electronic Supplementary Material Fig. S16).

FT-IR spectroscopy was used to elucidate the sensing mechanism of MH-5 for $Li^+$ ions (Fig. 6). Upon addition of $Li^+$, the peaks of -OH and -C–O–C at 3488 $cm^{-1}$ and 1103 $cm^{-1}$, respectively, shifted. These findings indicate that $Li^+$ ion interacts with the crown ether portion of MH-5 [59].

The sensing mechanism between MH-5 and $CN^-$ was elucidated through $^{13}C$ NMR titration experiments. In these experiments, $CN^-$ (dissolved in DMSO-d6) was added to a DMSO-d6 solution of MH-5, allowing for detailed observation of binding interactions. As illustrated in Fig. 7, the peak at 180 ppm belonging to the carbon numbered as C1 in the molecule shifted to 81.2 ppm after $CN^-$ was added. This is probably due to the conversion of C1 from $sp^2$ hybridization to $sp^3$ hybridization [60]. Moreover, a new peak at 118.2 ppm appeared, corresponding to $CN^-$ [61]. These results indicate a nucleophilic attack by $CN^-$ on the carbon atom (C1) of the indoline moiety [62, 63].

We also studied the reversibility of the binding of $Li^+$ and $CN^-$ by MH-5 in DMSO-PBS buffer (10 mM, pH = 7.25, v/v, 1:9), respectively. Ethylenediaminetetraacetic acid (EDTA) was used to remove $Li^+$ ion from the MH-5 + $Li^+$ [51]. As depicted in Fig. S17 of the Electronic Supplementary Material, the addition of EDTA led to a rapid increase in the fluorescence peak at 602 nm,

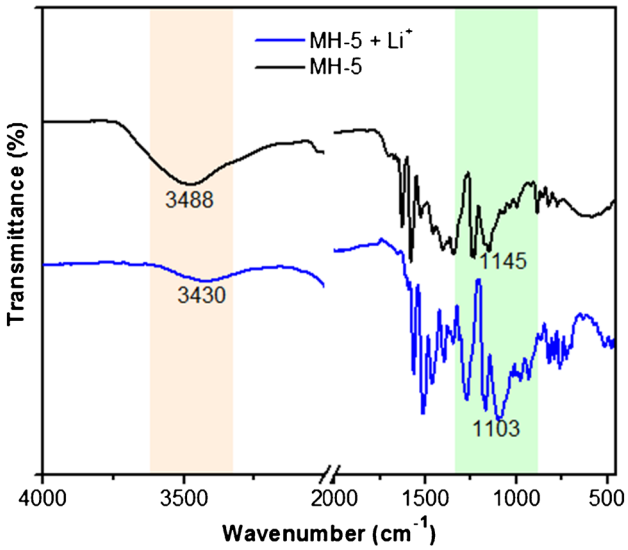


**Fig. 6** FT-IR spectra of MH-5 (black line) and MH-5 + $Li^+$ (blue line)

indicating that MH-5 can detect $Li^+$ through a reversible mechanism. On the other hand, trifluoroacetic acid (TFA) was used to remove the $CN^-$ ion from MH-5 + $CN^-$ [64]; however, as shown in Fig. S18 of the Electronic Supplementary Material, no significant change was observed in the fluorescence spectrum of MH-5 + $CN^-$. These results suggest an irreversible interaction between MH-5 and $CN^-$.

Based on the results obtained, the binding mechanisms of MH-5 between $Li^+$ and $CN^-$ were proposed as shown in Scheme 2. $CN^-$ detection was achieved through its nucleophilic addition to the indolium group of the sensor [65, 66], while $Li^+$ was detected by its coordination with

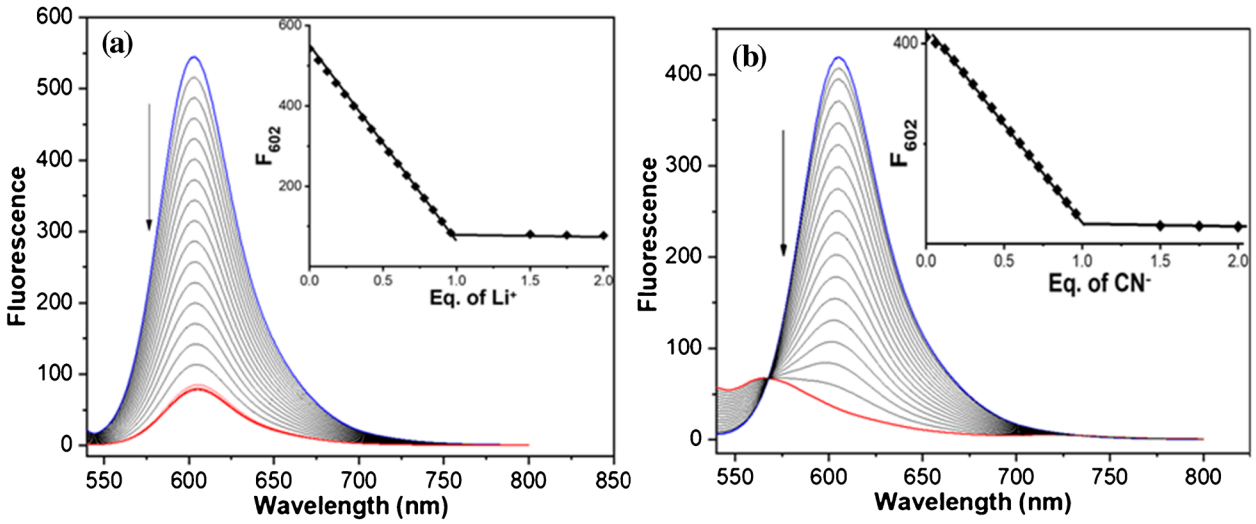


**Fig. 5** Fluorescence titration of 5.0 μM MH-5 with increasing concentrations (0, 0.3, 0.6, 0.9, 1.2, 1.5, 1.8, 2.1, 2.4, 2.7, 3.0, 3.3, 3.6, 3.9, 4.2, 4.5, 4.8, 5.0, 7.5, and 10 μM, respectively) in DMSO-PBS buffer (10 mM, pH = 7.25, v/v, 1:9) of $Li^+$ (**a**) and $CN^-$ (**b**)

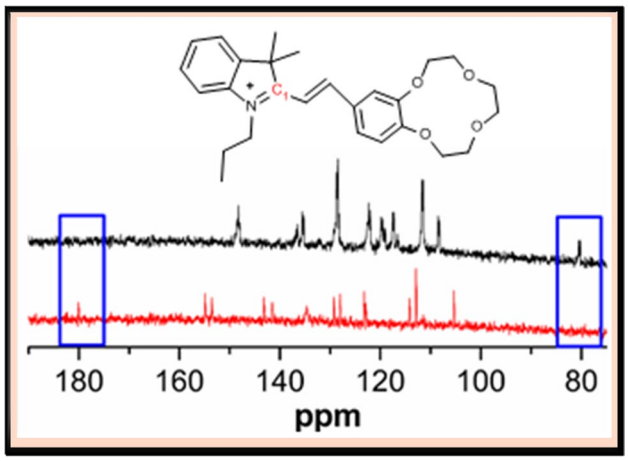


**Fig. 7** $^{13}C$ NMR spectra of MH-5 (red line) and in the presence of $CN^-$ (black line)

oxygen atoms in the crown ether moiety [47, 67]. In both detection mechanisms, the binding interactions with $Li^+$ and $CN^-$ induced fluorescence quenching in the fluorescence of MH-5.

To further confirm the binding mechanism between MH-5 and $Li^+/CN^-$, optimized structures of MH-5, MH-5 + $Li^+$, and MH-5 + $CN^-$ were obtained by density functional theory (DFT) calculations at the B3LYP/6-311G (d,p) level using the Gaussian 09 program [68]. As seen in Fig. 8, the orbital spatial distributions were found as − 8.60 eV/ − 5.63 eV (HOMO → LUMO) for MH-5, − 11.83 eV/ − 8.03 eV (HOMO → LUMO) for MH-5 + $Li^+$, and − 5.59 eV/ − 0.94 eV (HOMO-1 → LUMO) for MH-5 + $CN^-$. The energy gaps of MH-5, MH-5 + $Li^+$, and MH-5 + $CN^-$ were found as 2.97 eV, 3.82 eV, and 4.65 eV, respectively. The energy gaps of MH-5 + $Li^+$ and MH-5 + $CN^-$ were higher than that of MH-5. The increasing energy gap between the HOMO and LUMO induces a blue shift in the absorbance wavelength for both $Li^+$ and $CN^-$ [37, 69]. These results support the proposed mechanisms illustrated in Scheme 2.

## Detection limit studies

The detection limits for MH-5 with $Li^+$ and $CN^-$ ions were determined through absorption and fluorescence analyses across a concentration range of MH-5/$Li^+$ or $CN^-$ from 0.1 to 5.0 µM. Calibration curves were generated by applying linear regression to the relationship between $Li^+$ or $CN^-$ concentrations and the corresponding absorption or fluorescence intensities. Detection limits were then calculated using the formula $3\sigma/k$ [70–72], where $\sigma$ represents the standard deviation of blank signals from MH-5 (with $n = 10$) and $k$ denotes the slope of the calibration curves.

**Scheme 2.** Proposed response mechanisms of MH-5 toward $Li^+$ and $CN^-$

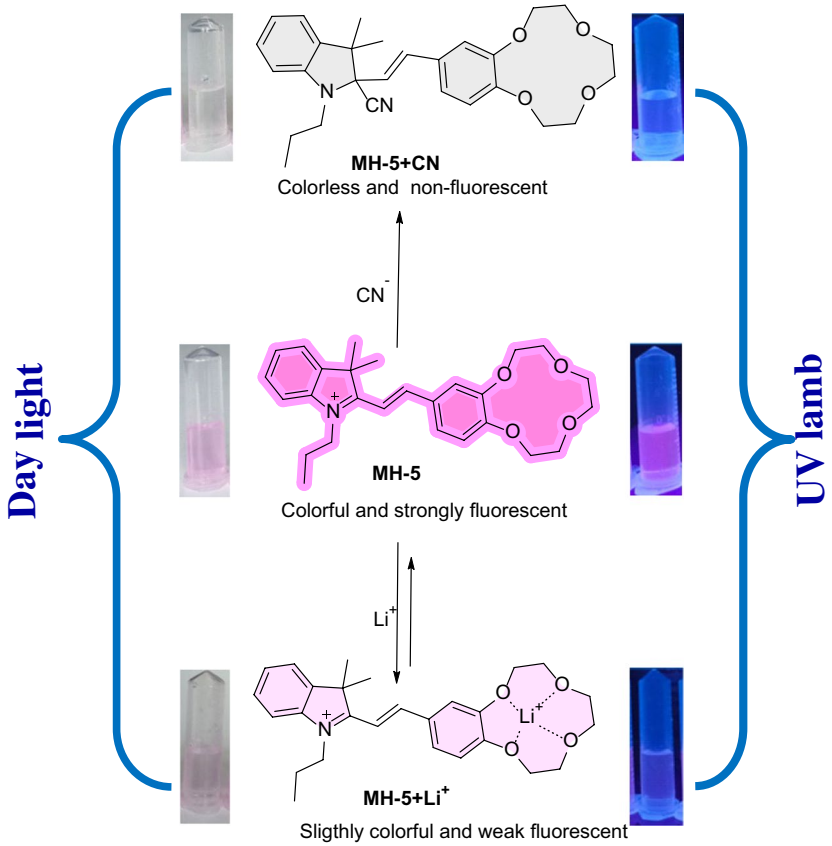

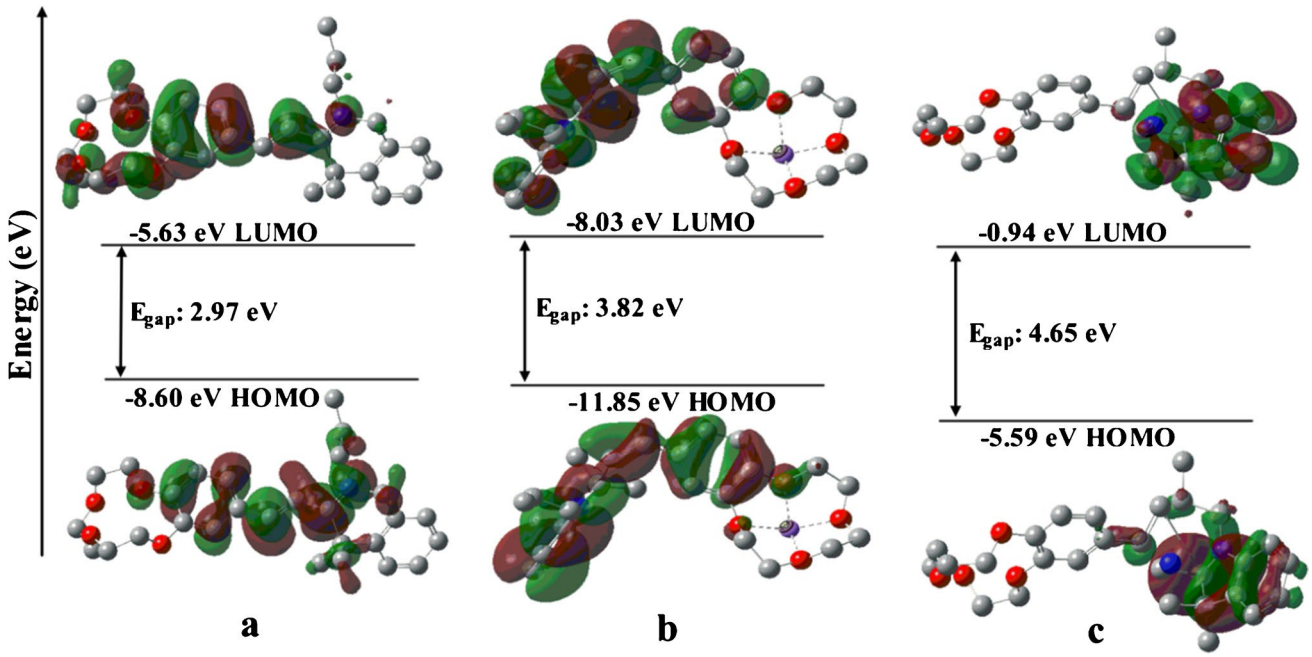


**Fig. 8** Energy diagrams of HOMO and LUMO orbitals: **a** MH-5, **b** MH-5 + $Li^+$, **c** MH-5 + $CN^-$

As depicted in Fig. S19 and Fig. S20 of the Electronic Supplementary Material, the calibration curves exhibit strong linear correlations between $CN^-$ concentrations and both absorbance and fluorescence intensities. The correlation coefficients are high, with $R^2 = 0.9971$ for the absorbance measurements ($y = -0.063x + 0.310$) and $R^2 = 0.9979$ for the fluorescence measurements ($y = -76.697x + 430.04$). The calculated detection limits were 0.355 µM for absorbance-based analysis and 0.154 µM for fluorescence-based analysis. Absorbance and fluorescence-based determination limit calculations were also performed for $Li^+$. As shown in Fig. S21 and Fig. S22 of the Electronic Supplementary Material, the calibration curves show good linear relationships between $Li^+$ concentration and absorbance/fluorescence intensities, with good correlation coefficients ($R^2 = 0.9982$, $y = -0.0512x + 0.3914$ from the absorbance measurements, $R^2 = 0.9991$, $y = -94.41x + 541.7$ from the fluorescence measurements). The detection limits were determined to be 0.189 µM for the absorbance-based study and to be 0.150 µM for the fluorescence-based study. The calculated detection limits for both $Li^+$ and $CN^-$ are below the concentration thresholds for these ions permitted in drinking water [4, 73].

### *Biological application of MH-5 in detecting $Li^+$ and $CN^-$*

The cytotoxic effect of the MH-5 material at different concentrations on HT-29 and L9-29 cell lines was investigated using the Alamar Blue assay [55, 56]. The MH-5 material induced 21.24% and 19.65% cell death rates in cancerous and healthy cell lines, respectively (Fig. 9). These cell death rates suggest that the material has relatively low or moderate toxicity. Cell death around 20% does not indicate high toxicity; however, it still shows an effect that warrants attention.

Even though we tested the toxicology of MH-5 on two different cell lines, HT-29 was chosen for cell imaging. The ability to detect $Li^+$ in live HT-29 was investigated

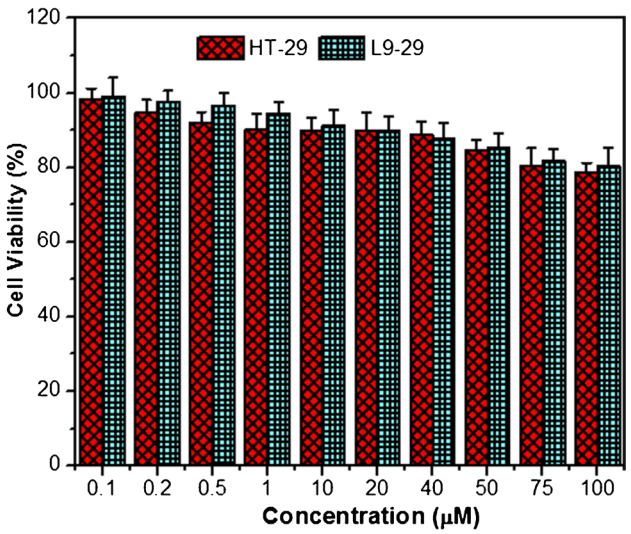


**Fig. 9** Cell viability (%) of the MH-5 on HT-29 and L9-29 cell lines. The error bars represent the mean ± SE of three independent measurements, with significance set at $p < 0.05$

using fluorescence microscopy. Live HT-29 cells incubated with 10 µM MH-5 showed weak fluorescence (Fig. 10b). From the merged image of the cell lines, it can be seen that MH-5 molecules can easily pass through the cell membrane (Fig. 10c) Then, the cells were loaded with $Li^+$. For $Li^+$ loading conditions, live HT-29 cells were incubated with 10 µ $LiNO_3$ at 37 °C for 4 h and then 10 µM MH-5 was added to the culture medium and incubated at 37 °C for 30 min. As seen in Fig. 10e, HT-29 cells incubated with $Li^+$ did not show fluorescence. The same experiments were carried out for $CN^-$ ions. The cells were loaded with $CN^-$. For $CN^-$ loading conditions, live HT-29 cells were incubated with 10 µ $CN^-$ at 37 °C for 4 h, and then 10 µM MH-5 was added to the culture medium and incubated at 37 °C for 30 min. As seen in Fig. 10h, HT-29 cells incubated with $CN^-$ did not show fluorescence. In general, it can be concluded that $Li^+$ and $CN^-$ ions in living cells are important molecules in selectivity by inhibiting the fluorescence properties of cell lines that are easily stained by the MH-5 chemosensor without damaging the cell lines.

### Comparison with previously reported sensors

The sensing ability of the present sensor toward $CN^-$ and $Li^+$ ions was also compared with others reported sensors in the literature, which is shown in Table S1. From the comparison, it is evident that the present sensor MH-5 has several advantages such as simple synthesis route, fast response time, low detection limit, and bio-imaging applications.

## Conclusion

In this study, a novel fluorescence sensor, MH-5, was successfully developed for the detection of $Li^+$ and $CN^-$ ions. The sensor was synthesized through a three-step process: a hemicyanine moiety was coupled with a crown ether moiety. Upon interaction with $Li^+$ and $CN^-$ ions, MH-5 exhibited distinct color changes from pink to pale pink and pink to colorless, respectively. The sensor demonstrated high selectivity and sensitivity, with significant absorbance and fluorescence quenching effects specific to $Li^+$ and $CN^-$, even in the presence of other tested cations and anions. Stoichiometric analysis revealed a 1:1 binding ratio between MH-5 and both $Li^+$ and $CN^-$ ions. The sensing mechanisms were also investigated using several analytical methods. The sensing mechanisms were verified with the NMR studies for $CN^-$ and the FT-IR studies for $Li^+$. For practical applications, MH-5 was further tested in living cells, where it efficiently permeated cell membranes and successfully visualized $Li^+$ and $CN^-$ ions. These findings suggest that MH-5 offers a promising approach for selective and effective

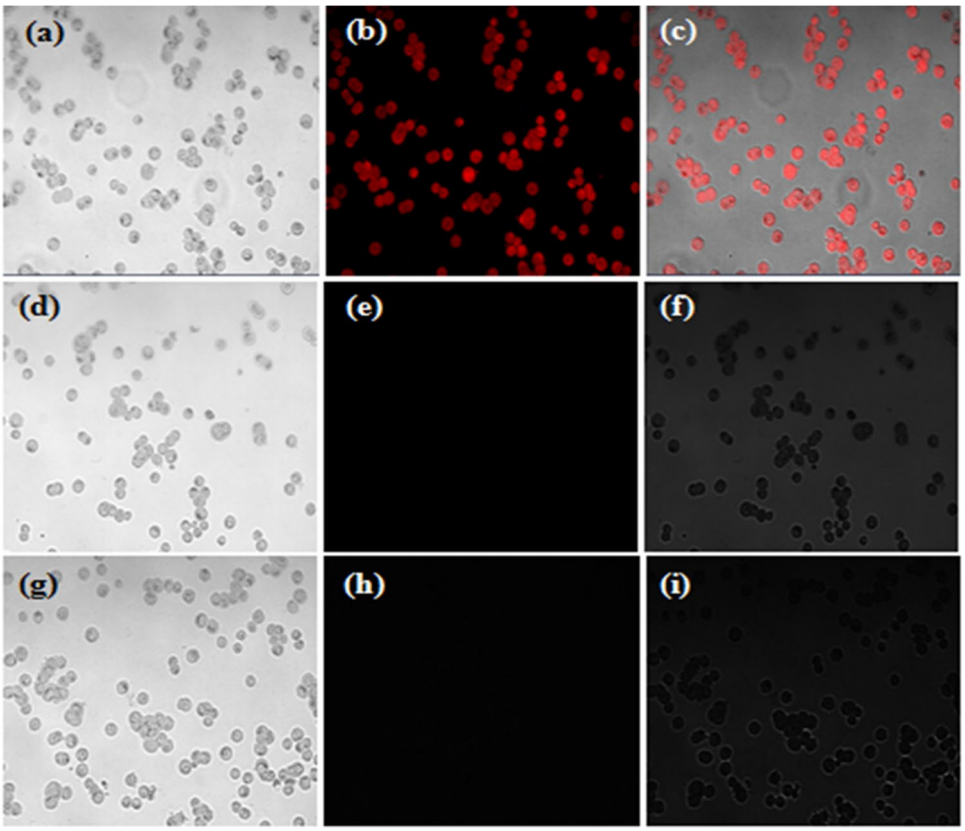


**Fig. 10** Fluorescence images of $Li^+$ and $CN^-$ with MH-5 in HT-29 cell lines. **a** Bright-field image of HT-29 cells incubated with MH-5 (10 µM). **b** The fluorescence image of HT-29 cells with MH-5. **c** Merged image of **a** and **b**. **d** Bright-field image of HT-29 cells pre-incubated with $LiNO_3$ (10 µM) and then incubated with MH-5 (10 µM). **e** The fluorescence image of HT-29 cells with $Li^+$ and MH-5. **f** Merged image of **d** and **e**. **g** Bright-field image of HT-29 cells pre-incubated with $CN^-$ (10 µM) and then incubated with MH-5 (10 µM). **h** The fluorescence image of HT-29 cells with $CN^-$ and MH-5. **i** Merged images of **g** and **h**

detection of $Li^+$ and $CN^-$ ions, with potential applicability in bio-imaging and diagnostic fields.

**Supplementary Information** The online version contains supplementary material available at https://doi.org/10.1007/s00216-025-05852-w.

**Acknowledgements** The authors are very grateful to Karamanoglu Mehmetbey University for their supports during the data collection and providing the Gaussian-9 data base and GaussView-5.0.8 software (KMU BAP 06-M-21) for this current work.

**Author contribution** ZA: conceptualization, investigation, writing—original draft, writing—review and editing. MK: investigation, methodology, visualization, writing—original draft. EA: investigation, validation, formal analysis. BYA: investigation, methodology, visualization, writing—original draft. MB: resources, supervision, writing—review and editing.

**Funding** Open access funding provided by the Scientific and Technological Research Council of Türkiye (TÜBİTAK).

**Data availability** All data are provided in full in the results section of this paper and supplementary information accompanying this paper.

## Declarations

**Conflict of interest** The authors declare no competing interests.



## References

1. Udhayakumari D. Chromogenic and fluorogenic chemosensors for lethal cyanide ion. A comprehensive review of the year 2016. Sens Actuators B: Chem. 2018;259:1022–57. https://doi.org/10.1016/j.snb.2017.12.006.
2. Jaszczak E, Polkowska Ż, Narkowicz S, Namieśnik J. Cyanides in the environment—analysis—problems and challenges. Environ Sci Pollut Res. 2017;24:15929–48. https://doi.org/10.1007/s11356-017-9081-7.
3. Halstrøm F, Møller KO. The content of cyanide in human organs from cases of poisoning with cyanide taken by mouth. With a contribution to the toxicology of cyanides. Acta Pharmacol Toxicol. 1945;1:18–28. https://doi.org/10.1111/j.1600-0773.1945.tb02560.x.
4. Kaloo MA, Sankar J. Reusable and specific proton transfer signalling by inorganic cyanide in solution and solid phase. Chem Commun. 2015;51:14528–31. https://doi.org/10.1039/C5CC05106A.
5. Thompson DT. Cyanide: Social, industrial and economic aspects. Gold Bull. 2001;34:133–133. https://doi.org/10.1007/BF03214826.
6. Sadyrbaeva TZh. Gold(III) recovery from non-toxic electrolytes using hybrid electrodialysis–electrolysis process. Sep Purif Technol. 2012;86:262–5. https://doi.org/10.1016/j.seppur.2011.10.007.
7. Citterio D, Takeda J, Kosugi M, Hisamoto H, Sasaki S, Komatsu H, et al. pH-Independent Fluorescent Chemosensor for Highly Selective Lithium Ion Sensing. Anal Chem. 2007;79:1237–42. https://doi.org/10.1021/ac061674g.
8. Mertens J, Wang Q-W, Kim Y, Yu DX, Pham S, Yang B, et al. Differential responses to lithium in hyperexcitable neurons from patients with bipolar disorder. Nature. 2015;527:95–9. https://doi.org/10.1038/nature15526.
9. Alda M. Lithium in the treatment of bipolar disorder: pharmacology and pharmacogenetics. Mol Psychiatry. 2015;20:661–70. https://doi.org/10.1038/mp.2015.4.
10. Priebe GA, Kanzawa MM. Reducing the progression of Alzheimer's disease in Down syndrome patients with micro-dose lithium. Med Hypotheses. 2020;137: 109573. https://doi.org/10.1016/j.mehy.2020.109573.
11. Mrozik W, Rajaeifar MA, Heidrich O, Christensen P. Environmental impacts, pollution sources and pathways of spent lithium-ion batteries. Energy Environ Sci. 2021;14:6099–121. https://doi.org/10.1039/D1EE00691F.
12. Martin G, Rentsch L, Höck M, Bertau M. Lithium market research – global supply, future demand and price development. Energy Storage Mater. 2017;6:171–9. https://doi.org/10.1016/j.ensm.2016.11.004.
13. Jing H, Wang F, Gao X. Lithium intoxication induced pyroptosis via / / inflammasome regulatory networks in kidney of mice. Environ Toxicol. 2022;37:825–35. https://doi.org/10.1002/tox.23446.
14. Ma J, Dasgupta PK. Recent developments in cyanide detection: A review. Anal Chim Acta. 2010;673:117–25. https://doi.org/10.1016/j.aca.2010.05.042.
15. Wen X, Ma P, Zhu G, Wu Z. Minimizing chemical interference errors for the determination of lithium in brines by flame atomic absorption spectroscopy analysis. Rare Met. 2006;25:309–15. https://doi.org/10.1016/S1001-0521(06)60059-4.
16. Virbickas P, Valiūnienė A, Baryševa D, Popkirov G, Ramanavičius A. Determination of cyanide concentration by chronoamperometry, cyclic voltammetry and fast Fourier transform electrochemical impedance spectroscopy. J Electroanal Chem. 2021;895: 115449. https://doi.org/10.1016/j.jelechem.2021.115449.
17. Huang X, Wang Z, Knibbe R, Luo B, Ahad SA, Sun D, et al. Cyclic voltammetry in lithium-sulfur batteries—challenges and opportunities. Energy Tech. 2019;7: 1801001. https://doi.org/10.1002/ente.201801001.
18. Suherman AL, Rasche B, Godlewska B, Nicholas P, Herlihy S, Caiger N, et al. Electrochemical detection and quantification of lithium ions in authentic human saliva using $LiMn_2O_4^-$ modified electrodes. ACS Sens. 2019;4:2497–506. https://doi.org/10.1021/acssensors.9b01176.
19. Aydin Z, Keskinates M, Yilmaz B, Durmaz M, Bayrakci M. A rapid responsive coumarin-naphthalene derivative for the detection of cyanide ions in cell culture. Anal Biochem. 2022;654: 114798. https://doi.org/10.1016/j.ab.2022.114798.
20. Yilmaz B, Keskinates M, Aydin Z, Bayrakci M. A highly selective optical sensor for the detection of cyanide ions in aqueous solution and living cells. J Photochem Photobiol. 2022;424: 113651. https://doi.org/10.1016/j.jphotochem.2021.113651.
21. Chakraborty S, Paul S, Roy P, Rayalu S. Detection of cyanide ion by chemosensing and fluorosensing technology. Inorg Chem Commun. 2021;128: 108562. https://doi.org/10.1016/j.inoche.2021.108562.
22. Rajpurohit D, Sharma P, Bathvar H, Syed S, Shrivastav PS. Lithium selective receptors. Coord Chem Rev. 2024;515: 215968. https://doi.org/10.1016/j.ccr.2024.215968.

23. Yin J, Hu Y, Yoon J. Fluorescent probes and bioimaging: alkali metals, alkaline earth metals and pH. Chem Soc Rev. 2015;44:4619–44. https://doi.org/10.1039/C4CS00275J.
24. Immanuel David C, Lee H. Cutting-edge advances in colorimetric and fluorescent chemosensors for detecting lethal cyanide ion: A comprehensive review. Microchem J. 2024;200: 110359. https://doi.org/10.1016/j.microc.2024.110359.
25. Gul Z, Iqbal A, Shoukat J, Anila A, Rahman R, Ullah S, et al. Nanoparticles based sensors for cyanide ion sensing, basic principle, mechanism and applications. Crit Rev Anal Chem. 2023;1–15. https://doi.org/10.1080/10408347.2023.2295511.
26. Pati PB. Organic chemodosimeter for cyanide: A nucleophilic approach. Sens Actuators B: Chem. 2016;222:374–90. https://doi.org/10.1016/j.snb.2015.08.044.
27. Bencini A, Lippolis V. Metal-based optical chemosensors for $CN^-$ detection. Environ Sci Pollut Res. 2016;23:24451–75. https://doi.org/10.1007/s11356-016-7419-1.
28. Dharaniprabha V, Kalavathi A, Satheeshkumar K, Elango KP. A ferrocene-based chemo-dosimeter for colorimetric and electrochemical detection of cyanide and its estimation in cassava flour. Anal Methods. 2024;16:4880–8. https://doi.org/10.1039/D4AY00415A.
29. Jamuna K, Gayathri S, Sivakumar S, Ashokkumar B. Design and development of a fluorometric and colorimetric sensor for toxic cyanide detection by pyridinium scaffolds: live cell imaging and real sample analysis. Sens Diagn. 2023;2:337–46. https://doi.org/10.1039/D2SD00163B.
30. Nelson M, Ayyanar S, Selvaraj M, Assiri MA. Exploiting cyanide anion detection in food samples and for constructing logic gates by turn-off fluorescent chemosensor. J Mol Struct. 2025;1321: 140018. https://doi.org/10.1016/j.molstruc.2024.140018.
31. Tigreros A, Castillo J-C, Portilla J. Cyanide chemosensors based on 3-dicyanovinylpyrazolo[1,5-a]pyrimidines: Effects of peripheral 4-anisyl group substitution on the photophysical properties. Talanta. 2020;215: 120905. https://doi.org/10.1016/j.talanta.2020.120905.
32. Wang L, Li L, Cao D. A BODIPY-based dye with red fluorescence in solid state and used as a fluorescent and colorimetric probe for highly selective detection of cyanide. Sens Actuators B: Chem. 2017;239:1307–17. https://doi.org/10.1016/j.snb.2016.09.112.
33. Yu Y, Shu T, Yu B, Deng Y, Fu C, Gao Y, et al. A novel turn-on fluorescent probe for cyanide detection in aqueous media based on a BODIPY-hemicyanine conjugate. Sens Actuators B: Chem. 2018;255:3170–8. https://doi.org/10.1016/j.snb.2017.09.142.
34. Gwon S-Y, Lee E-M, Kim S-H. Hemicyanine-based colorimetric chemosensors: Different recognition mechanisms for CN− sensing. Spectrochim Acta A Mol Biomol Spectrosc. 2012;96:77–81. https://doi.org/10.1016/j.saa.2012.05.018.
35. Liu S, Yang M, Liu Y, Chen H, Li H. A novel "turn-on" fluorescent probe based on triphenylimidazole-hemicyanine dyad for colorimetric detection of $CN^-$ in 100% aqueous solution. J Hazard Mater. 2018;344:875–82. https://doi.org/10.1016/j.jhazmat.2017.11.042.
36. Said AI, Kandinska M, Vasilev A, Grabchev I. Styryl hemicyanine-DNA assembly for selective $Hg^{2+}$ sensing and molecular computing. J Photochem Photobiol. 2024;452: 115590. https://doi.org/10.1016/j.jphotochem.2024.115590.
37. Ranolia A, Sindhu J, Kumar P, Kumar S. Divulging indolium inspired cyanide sensors: Did it win the throne? Coord Chem Rev. 2024;498:215463. https://doi.org/10.1016/j.ccr.2023.215463.
38. Javanbakht F, Najafi H, Jalili K, Salami-Kalajahi M. A review on photochemical sensors for lithium ion detection: relationship between the structure and performance. J Mater Chem A. 2023;11:26371–92. https://doi.org/10.1039/D3TA06113B.
39. Kim H, Koo B. Lithium sensors based on photophysical changes of 1-aza-12-crown-4 naphthalene derivatives synthesized *via* Buchwald-Hartwig amination. RSC Adv. 2022;12:31976–84. https://doi.org/10.1039/D2RA05746H.
40. Fan J, Hu M, Zhan P, Peng X. Energy transfer cassettes based on organic fluorophores: construction and applications in ratiometric sensing. Chem Soc Rev. 2013;42:29–43. https://doi.org/10.1039/C2CS35273G.
41. Villemin E, Raccurt O. Optical lithium sensors. Coord Chem Rev. 2021;435: 213801. https://doi.org/10.1016/j.ccr.2021.213801.
42. Kamenica M, Kothur R, Willows A, Patel B, Cragg P. Lithium Ion Sensors. Sensors. 2017;17:2430. https://doi.org/10.3390/s17102430.
43. Richards RA, Hammons K, Joe M, Miskelly GM. Observation of a Stable Water-Soluble Lithium Porphyrin. Inorg Chem. 1996;35:1940–4. https://doi.org/10.1021/ic941434w.
44. Tabata M, Nishimoto J, Kusano T. Spectrophotometric determination of lithium ion using a water-soluble octabromoporphyrin in aqueous solution. Talanta. 1998;46:703–9. https://doi.org/10.1016/S0039-9140(97)00327-5.
45. Obare SO, Murphy CJ. A Two-Color Fluorescent Lithium Ion Sensor. Inorg Chem. 2001;40:6080–2. https://doi.org/10.1021/ic010271q.
46. Gulino A, Lupo F, Cristaldi DA, Pappalardo S, Capici C, Gattuso G, et al. A Viable Route for Lithium Ion Detection. Eur J Inorg Chem. 2014;2014:442–9. https://doi.org/10.1002/ejic.201301213.
47. Kumar M, Kumar N, Bhalla V. Thiacalix[4]crown based optical chemosensor for Fe3+, Li+ and cysteine: a Fe3+ /Li+ ion synchronized allosteric regulation. Dalton Trans. 2013;42:981–6. https://doi.org/10.1039/C2DT31940C.
48. Kang J, Li E, Cui L, Shao Q, Yin C, Cheng F. Lithium ion specific fluorescent reversible extraction-release based on spiropyran isomerization combining crown ether coordination and its bioimaging. Sens Actuators B: Chem. 2021;327: 128941. https://doi.org/10.1016/j.snb.2020.128941.
49. Ando Y, Hiruta Y, Citterio D, Suzuki K. A highly $Li^+$-selective glass optode based on fluorescence ratiometry. Analyst. 2009;134:2314. https://doi.org/10.1039/b912756a.
50. Sprenger T, Schwarze T, Müller H, Sperlich E, Kelling A, Holdt H, et al. BODIPY-Equipped Benzo-Crown-Ethers as Fluorescent Sensors for pH Independent Detection of Sodium and Potassium Ions. ChemPhotoChem. 2023;7: e202200270. https://doi.org/10.1002/cptc.202200270.
51. Hangarge RV, La DD, Boguslavsky M, Jones LA, Kim YS, Bhosale SV. An Aza-12-crown-4 Ether-Substituted Naphthalene Diimide Chemosensor for the Detection of Lithium Ion. ChemistrySelect. 2017;2:11487–91. https://doi.org/10.1002/slct.201702085.
52. Kumari S, Joshi S, Sarmah A, Pant D, Sakhuja R. Highly Selective Sensing of $Li^+$ in H2O/CH3CN via Fluorescence 'Turn-on' Response of a Coumarin-Indole Linked Dyad: an Experimental and Theoretical Study. J Fluoresc. 2016;26:2177–85. https://doi.org/10.1007/s10895-016-1913-1.
53. Tomar K, Ramanathan G. New self-assembled archetypes in crown ether substituted Δ^Z Phe containing tripeptides. J Chem Sci. 2019;131:47. https://doi.org/10.1007/s12039-019-1623-8.
54. Samanta A, Vendrell M, Das R, Chang Y-T. Development of photostable near-infrared cyanine dyes. Chem Commun. 2010;46:7406. https://doi.org/10.1039/c0cc02366c.
55. Keskinates M, Aydin Z, Yilmaz Altinok B, Bayrakci M. A turn-off fluorescent sensor based on Schiff base incorporating diformyl phenol moiety for the detection of $Cu^{2+}$ in aqueous solution at nanomolar level and its application in living cells. J Photochem Photobiol. 2024;455: 115765. https://doi.org/10.1016/j.jphotochem.2024.115765.

56. Yilmaz B, Keskinates M, Bayrakci M. Novel integrated sensing system of calixarene and rhodamine molecules for selective colorimetric and fluorometric detection of $Hg^{2+}$ ions in living cells. Spectrochim Acta A Mol Biomol Spectrosc. 2021;245: 118904. https://doi.org/10.1016/j.saa.2020.118904.
57. Hazra A, Ghosh P, Roy P. A rhodamine based dual chemosensor for $Al^{3+}$ and $Hg^{2+}$: Application in the construction of advanced logic gates. Spectrochim Acta A Mol Biomol Spectrosc. 2022;271: 120905. https://doi.org/10.1016/j.saa.2022.120905.
58. Aydin Z, Keleş M. Colorimetric cadmium ion detection in aqueous solutions by newly synthesized Schiff bases. Turk J Chem. 2020;44:791–804. https://doi.org/10.3906/kim-1912-36.
59. Bezdomnikov AA, Demina LI, Kuz'mina LG, Kostikova GV, Zhilov VI, Tsivadze AY. Study of lithium-extraction systems based on Benzo-15-Crown-5 ether and Alkylimidazolium-Based Ionic Liquid. Molecules. 2023;28:935. https://doi.org/10.3390/molecules28030935.
60. Buinauskaitė V, Martynaitis V, Mangelinckx S, Kreiza G, De Kimpe N, Šačkus A. Facile synthesis of spiro[benzo[e]indole-2,2′-piperidine] derivatives and their transformation to novel fluorescent scaffolds. Tetrahedron. 2012;68:9260–6. https://doi.org/10.1016/j.tet.2012.08.073.
61. Maurya N, Kumar SA. A chromogenic and fluorogenic chemodosimeter for selective detection of $CN^-$. Inorganica Chim Acta. 2020;499: 119156. https://doi.org/10.1016/j.ica.2019.119156.
62. Mahapatra AK, Maiti K, Manna SK, Maji R, Mukhopadhyay CD, Pakhira B, et al. Unique Fluorogenic Ratiometric Fluorescent Chemodosimeter for Rapid Sensing of $CN^-$ in Water. Chem Asian J. 2014;9:3623–32. https://doi.org/10.1002/asia.201402923.
63. Lyngdoh Lyngkhoi D, Khatua S. A coumarin containing hemicyanine-based probe for dual channel detection of cyanide ion. Inorganica Chim Acta. 2024;572: 122300. https://doi.org/10.1016/j.ica.2024.122300.
64. Kumar A, Jeong E, Noh Y, Chae PS. Fluorescence-based ratiometric sensors as emerging tools for $CN^-$ detection: Chemical structures, sensing mechanisms and applications. Methods. 2024;222:57–80. https://doi.org/10.1016/j.ymeth.2024.01.001.
65. Wang S, Fei X, Guo J, Yang Q, Li Y, Song Y. A novel reaction-based colorimetric and ratiometric fluorescent sensor for cyanide anion with a large emission shift and high selectivity. Talanta. 2016;148:229–36. https://doi.org/10.1016/j.talanta.2015.10.058.
66. Li J, Qi X, Wei W, Zuo G, Dong W. A red-emitting fluorescent and colorimetric dual-channel sensor for cyanide based on a hybrid naphthopyran-benzothiazol in aqueous solution. Sens Actuators B: Chem. 2016;232:666–72. https://doi.org/10.1016/j.snb.2016.04.021.
67. Gao Y, Zhong R-L, Xu H-L, Sun S-L, Su Z-M. The effect of ring sizes and alkali metal cations on interaction energy, charge transfer and nonlinear optical properties of crown ether derivatives. RSC Adv. 2015;5:30107–19. https://doi.org/10.1039/C5RA01145K.
68. Frisch MJ, Trucks GW, Schlegel HB, Scuseria GE, Robb MA, Cheeseman JR, Scalmani G, Barone V, Mennucci B, Petersson GA, Nakatsuji H, Caricato M, Li X, Hratchian HP, Izmaylov AF, Bloino J, Zheng G, Sonnenberg JL, Hada M, Ehara M, Toyota K, Fukuda R, Hasegawa J, Ishida M, Nakajima T, Honda Y, Kitao O, Nakai H, Vreven T, Montgomery JA Jr., Peralta JE, Ogliaro F, Bearpark M, Heyd JJ, Brothers E, Kudin KN, Staroverov VN, Kobayashi R, Normand J, Raghavachari K, Rendell A, Burant JC, Iyengar SS, Tomasi J, Cossi M, Rega N, Millam JM, Klene M, Knox JE, Cross JB, Bakken V, Adamo C, Jaramillo J, Gomperts R, Stratmann RE, Yazyev O, Austin AJ, Cammi R, Pomelli C, Ochterski JW, Martin RL, Morokuma K, Zakrzewski VG, Voth GA, Salvador P, Dannenberg JJ, Dapprich S, Daniels AD, Farkas Ö, Foresman BJ, Ortiz JV, Cioslowski J, Fox DJ (2009) Gaussian 09 Revision A.02. Gaussian, Inc., Wallingford, CT
69. Doyuran B, Gökoğlu E, Zouitini A, Keleş E, Taskin-Tok T, Seferoğlu N, et al. A Novel Fluorescent Probe for the Detection of Cyanide Ions in Solutions and Studies on Its Biophysical Interactions with ctDNA and Proteases. J Fluoresc. 2022;32:2173–88. https://doi.org/10.1007/s10895-022-03014-0.
70. Aydin Z. A novel phenanthroline-based colorimetric turn-off optical sensor for $Zn^{2+}$. Inorg Chim Acta. 2021;517: 120200. https://doi.org/10.1016/j.ica.2020.120200.
71. Aydin Z, Keles M. Highly selective Schiff base derivatives for colorimetric detection of $Al^{3+}$. Turk J Chem. 2017;41:89–98. https://doi.org/10.3906/kim-1603-127.
72. Aydin Z, Keskinates M, Yilmaz B, Bayrakci M. An isonicotinohydrazide based fluorescence sensor for detection of $Zn^{2+}$ in biological systems: Experimental and theoretical studies along with cell imagine. Inorg Chim Acta. 2023;557: 121680. https://doi.org/10.1016/j.ica.2023.121680.
73. Vesković J, Miletić A, Lučić M, Onjia A. Appraisal of contamination, hydrogeochemistry, and Monte Carlo simulation of health risks of groundwater in a lithium-rich ore area. Environ Geochem Health. 2024;46:468. https://doi.org/10.1007/s10653-024-02257-z.